Calcium-Dependent Heme Structure in the Reduced Forms of the Bacterial Cytochrome *c* Peroxidase from *Paracoccus pantotrophus*†

Sofia R. Pauleta,*,‡ Yi Lu,§ Celia F. Goodhew,|| Isabel Moura,‡ Graham W. Pettigrew,|| and John A. Shelnutt*,§

REQUIMTE/CQFB, Departamento de Química, Faculdade de Ciências e Tecnologia, Universidade Nova de Lisboa, 2829-516 Caparica, Portugal, Nanomaterials Sciences Department, Sandia National Laboratories, Albuquerque, New Mexico 87185-1349, Department of Chemistry, University of Georgia, Athens, Georgia 30602-2556, and Royal (Dick) School of Veterinary Studies, University of Edinburgh, Summerhall, Edinburgh EH9 1QH, U.K.

Received December 20, 2007; Revised Manuscript Received April 5, 2008

ABSTRACT: This work reports for the first time a resonance Raman study of the mixed-valence and fully reduced forms of *Paracoccus pantotrophus* bacterial cytochrome *c* peroxidase. The spectra of the active mixed-valence enzyme show changes in the structure of the ferric peroxidatic heme compared to the fully oxidized enzyme; these differences are observed upon reduction of the electron-transferring heme and upon full occupancy of the calcium site. For the mixed-valence form in the absence of Ca^{2+}, the peroxidatic heme is six-coordinate and low-spin on the basis of the frequencies of the structure-sensitive Raman lines: the enzyme is inactive. With added Ca^{2+}, the peroxidatic heme is five-coordinate high-spin and active. The calcium-dependent spectral differences indicate little change in the conformation of the ferrous electron-transferring heme, but substantial changes in the conformation of the ferric peroxidatic heme. Structural changes associated with Ca^{2+} binding are indicated by spectral differences in the structure-sensitive marker lines, the out-of-plane low-frequency macrocyclic modes, and the vibrations associated with the heme substituents of that heme. The Ca^{2+}-dependent appearance of a strong γ_{15} saddling-symmetry mode for the mixed-valence form is consistent with a strong saddling deformation in the active peroxidatic heme, a feature seen in the Raman spectra of other peroxidases. For the fully reduced form in the presence of Ca^{2+}, the resonance Raman spectra show that the peroxidatic heme remains high-spin.

Hydrogen peroxide is a toxic compound produced in the cells by the incomplete reduction of oxygen during oxidative metabolism. Its toxicity is due to its tendency to produce free radicals that can lead to cell damage or death (*1*). In most living cells, it can be removed enzymatically by catalases or peroxidases. While catalase disproportionates peroxide into water and oxygen, peroxidase reduces peroxide to water using a variety of oxidizable substrates. In the case of the bacterial cytochrome *c* peroxidases (BCCP),[1] the oxidizable substrates are the monoheme *c*-type cytochromes or type 1 copper proteins, like azurin (*2*) or pseudoazurin (*3*).

The bacterial cytochrome *c* peroxidases are periplasmic enzymes that contain two covalently bound *c*-type hemes. They have been isolated from several organisms, including *Pseudomonas aeruginosa* (*4*), *Rhodobacter capsulatus* (*5, 6*), *Nitrosomonas europaea* (*7*), *Pseudomonas nautica* (*8*), *Pseudomonas stutzeri* (*9*), *Methylococcus capsulatus* (*10*), and *Paracoccus pantotrophus* (*11*). The two most studied enzymes are the ones isolated from *P. pantotrophus* and *Ps. aeruginosa*. The three-dimensional structure of *P. pantotrophus* bacterial cytochrome *c* peroxidase in two redox states was recently determined (*12*). The overall structure of the enzyme is very similar in both redox states (fully oxidized and mixed-valence), containing two domains each with one heme (shown schematically in Figure 1). In the fully oxidized form, the N-terminal domain contains a bis-histidine low-potential (LP) heme and the C-terminal domain contains a high-potential (HP) heme coordinated by methionine and histidine residues. In the mixed-valence form, the C-terminal heme is reduced and the N-terminal heme is five-coordinate (*12*). The C-terminal heme has been proposed to be the electron-transferring heme, acting as the source of one electron for the reduction of peroxide, while the latter acts as the peroxidatic heme and gives the second electron.

The activity of the *Paracoccus* enzyme is dependent on two factors. The enzyme must contain calcium ion, and the electron-transferring heme must be reduced (*13*). In addition, the calcium ion promotes dimerization of the enzyme, and this is also dependent on protein concentration. Thus, dilution of the enzyme results in loss of activity. As mentioned, the configurations of the heme groups and active site change

† Sandia National Laboratories is a multiprogram laboratory operated by Sandia Corp., a Lockheed Martin company, for the U.S. Department of Energy's National Nuclear Security Administration under Contract DEAC04-94AL85000. S.R.P. and I.M. thank the Fundação para a Ciência e Tecnologia for financial support.

* To whom correspondence should be addressed. S.R.P.: REQUIMTE-CQFB, Dep. Química, FCT-UNL, 2829-516 Caparica, Portugal; e-mail, srp@dq.fct.unl.pt. J.A.S.: Sandia National Laboratories, 1001 University Blvd. SE, Albuquerque, NM 87106; phone, (505) 272-7160; fax, (505) 272-7077; e-mail, jasheln@unm.edu.

‡ Universidade Nova de Lisboa.

§ Sandia National Laboratories and University of Georgia.

|| University of Edinburgh.

[1] Abbreviations: ASC, ascorbate; BCCP, bacterial cytochrome *c* peroxidase; DAD, diaminodurol; EGTA, ethylene glycol bis(β-aminoethyl ether) *N*,*N*,*N*′,*N*′-tetraacetic acid; HP, high-potential; LP, low-potential; P, peroxidatic; E, electron-transferring; *Pa-p*, *Paracoccus pantotrophus*; *Ps-a*, *Pseudomonas aeruginosa*; RR, resonance Raman.

10.1021/bi702486d CCC: $40.75
Published on Web 04/29/2008

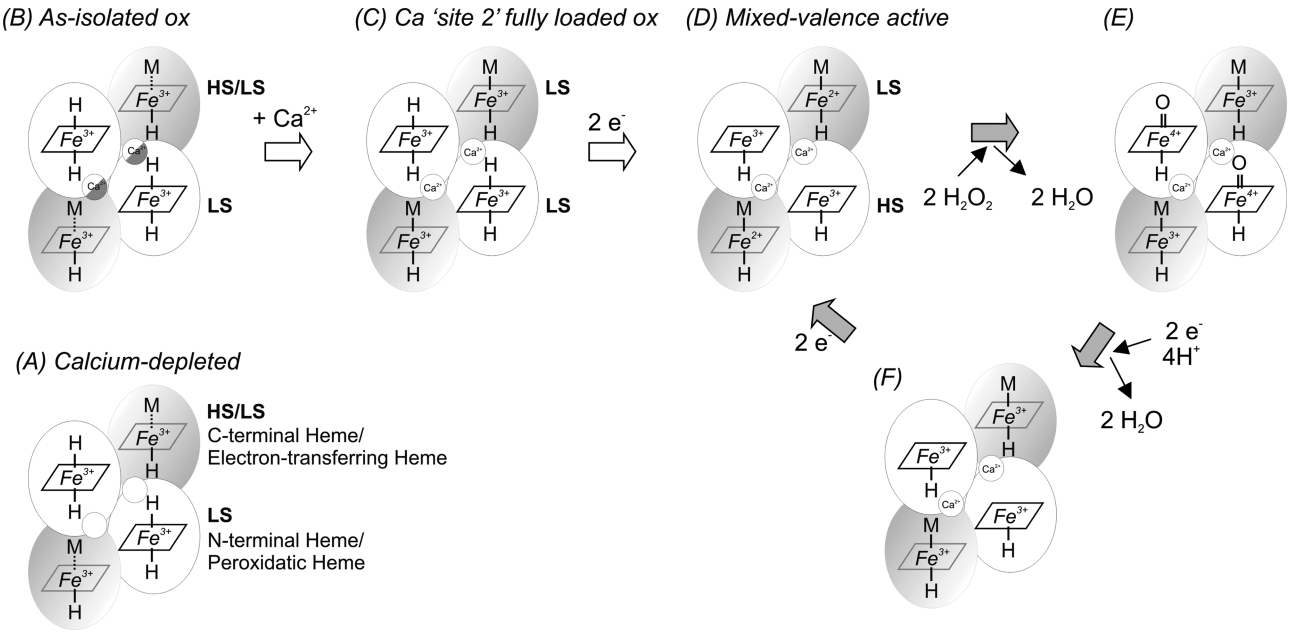

FIGURE 1: Proposed mechanism and different protein forms existing under various states of reduction and calcium ion concentrations at pH 7.5. (A) Ca-depleted oxidized BCCP. The partially filled calcium "site 2", present in the oxidized as-isolated BCCP (state B), can be completely filled by the addition of calcium ions (state C). After the reduction of the high-potential heme (mixed-valence state), the enzyme becomes active (state D) and able to react with hydrogen peroxide (state E). The catalytic cycle (gray arrows) is complete after the delivery of two consecutive electrons (from state E to F and then to D) and returns to the initial state D. The calcium site represented is site 2. The location of calcium "site 1" is not known.

upon reduction of the high-potential (electron-transferring) heme. Specifically, the high-potential heme, which exhibits a high-spin−low-spin equilibrium in the fully oxidized form of the enzyme, becomes fully low-spin when reduced. In the presence of calcium ions, the reduction of the high-potential heme also causes the low-potential ferric heme to change from low-spin to high-spin and to lose a histidine ligand, opening a coordination site to H_2O_2.

The calcium ions play a pivotal role in the activation of the enzyme, probably by enabling the structural changes that occur at the peroxidatic heme. Some of the proposed protein species that differ in oxidation state, coordination state, spin state, and occupation of the calcium-binding site are illustrated in Figure 1.

Paracoccus cytochrome *c* peroxidase has been studied using several techniques, but resonance Raman spectroscopy has been shown to be most helpful in elucidating the effect of the calcium ions on the detailed structure of the hemes (*14*). Raman lines corresponding to the vibrations of the heme are observed without interference from the rest of the protein because of resonance enhancement of the spectrum of the heme groups. For excitation using laser wavelengths in the visible region where the heme absorbs light, the enhanced Raman lines are entirely those of the porphyrin macrocycle vibrations, substituent groups on the macrocycle, and the axial ligands. Both in-plane and out-of-plane vibrations of the macrocycle are Raman active, the latter mostly as a result of out-of-plane distortion of the macrocycle that is induced by the protein surrounding the heme. Changes in these Raman active modes have provided a detailed picture of the structural changes caused by calcium ion binding to the fully oxidized *P. pantotrophus* enzyme (*14*).

Here we report for the first time the resonance Raman (RR) spectra of the mixed-valence and the fully reduced forms of a bacterial cytochrome *c* peroxidase. The RR spectra reveal the conformational changes of the hemes and their substituents that are associated with heme reduction, the binding of calcium ions, and the activation of the enzyme. In addition, under conditions for which the enzyme is active (i.e., in the mixed-valence form and in the presence of Ca^{2+}), the RR spectrum of one of the hemes becomes typical of that of other peroxidases, that is, five-coordinate, high-spin, and saddled. The RR spectra also prove many of the effects of reduction and calcium ion binding on the coordination and spin states of the hemes of the enzyme that were predicted by other methods. Moreover, the RR showed for the first time that, in the fully reduced form of the enzyme, the low-potential heme is high-spin.

MATERIALS AND METHODS

Purification of Cytochrome c Peroxidase. Cytochrome *c* peroxidase was purified from *P. pantotrophus* LMD 52.44 as previously described (*11*). Concentrated stocks of protein in 5 mM MES (pH 6.0) and 10 mM NaCl were stored at −40 °C. The enzyme concentration was determined, in the oxidized state, using an extinction coefficient at 408 nm for the monomer of 250 mM^{-1} cm^{-1}.

Preparation of Cytochrome c Peroxidase for RR Spectroscopy. A Centricon apparatus was used to change the buffer of the protein to 5 mM HEPES and 10 mM NaCl (pH 7.5) and to concentrate the solution to give a stock solution in this buffer. For the RR experiments, BCCP was diluted from the stock solution in 5 mM HEPES and 10 mM NaCl (pH 7.5) to 50 μM in the same buffer and aged for 60 min at 4 °C. The protein fully loaded with Ca^{2+} was obtained by adding $CaCl_2$ to a concentration of 2 mM, and the solution was aged for 60 min at 4 °C prior to the RR experiments. To produce the protein with Mg^{2+}, $MgCl_2$ was added to a concentration of 2 mM and the solution aged for 60 min at

4 °C. The protein depleted of calcium was obtained by incubating the BCCP with EGTA (2 mM) for 60 min at 4 °C. The BCCP was then reduced to the mixed-valence form by adding ascorbate and DAD to concentrations of 1 mM and 5 μM, respectively, and the RR spectra were collected after incubation for 2−30 min to check that attainment of a stable state. The fully reduced protein was obtained by adding sodium dithionite. The fully oxidized samples were prepared as described previously using ferricyanide (*14*). The enzyme exhibits a monomer−dimer equilibrium that is dependent not only on the presence of calcium ions but also on pH, ionic strength, and protein concentration (*15*). In the as-isolated oxidized state at a protein concentration of 10 μM, an ionic strength of 10 mM, and pH 7.5, the protein is largely monomeric, contains a calcium ion in what has been called site 1, but lacks calcium ion in the key site 2 binding site which is linked both to the spin-state change in the mixed-valence enzyme and to activity (*16*). However, at the protein concentration of 50 μM required for Raman spectroscopy, site 2 is partially occupied in the as-isolated enzyme.

The resonance Raman spectra were acquired at pH 7.5 instead of pH 6.0, due to the higher occupancy of the calcium site 2 at pH 6.0, which would lead to complication of the spectra and their interpretation. An additional advantage is that the calcium chelation ability of EGTA is much greater at pH 7.5 than at pH 6.0.

Resonance Raman Spectroscopy. RR spectra were recorded using the 406.7 nm line of an INNOVA Kr^+ laser (Coherent) and a Raman spectrometer described previously (*14*). Briefly, the spectrometer is a 0.75 m monochromator (Instruments, SA) with a CCD detector. The slit width of 100 μm gives a spectral resolution of 2 cm^{-1}. Position mode was used for detection with each section covering 500 cm^{-1} of the Raman spectrum without moving the grating. Spectra were output from the CCD and its computer controller for plotting with SigmaPlot (SPSS). Polarized spectra were obtained using an oriented Polaroid sheet located between the notch filter (Kaiser Optical Systems) and a polarization scrambler in front of the entrance slit. For the polarized spectra, spectral decompositions (not shown) were accomplished using Voigt line shapes with PeakFit (SPSS) in some cases.

Raman samples were kept in ice until the spectra were obtained, typically at room temperature (25 °C) for 2−10 min using less than 30 mW of power in a partially focused beam.

RESULTS

The Raman spectra of mixed-valence and fully reduced *Pa-p* BCCP were obtained with 406.7 nm laser excitation (near the Soret band) (visible spectra shown in Figure S1-A, inset, of the Supporting Information). Soret band excitation enhances mostly polarized totally symmetric A_{1g} and depolarized dynamic Jahn−Teller-active B_{1g} and B_{2g} in-plane vibrational modes, which are particularly evident in the high-frequency region of the Raman spectra (Figures 2A, 3, S1A, S2A, and S3A). Here, the polarization and symmetry properties are indicated by the square-planar D_{4h}-symmetric notations. The frequencies of several high-frequency modes of these symmetry types, including ν_4 (A_{1g}), ν_3 (A_{1g}), ν_2 (A_{1g}), and ν_{10} (B_{1g}), are known to be

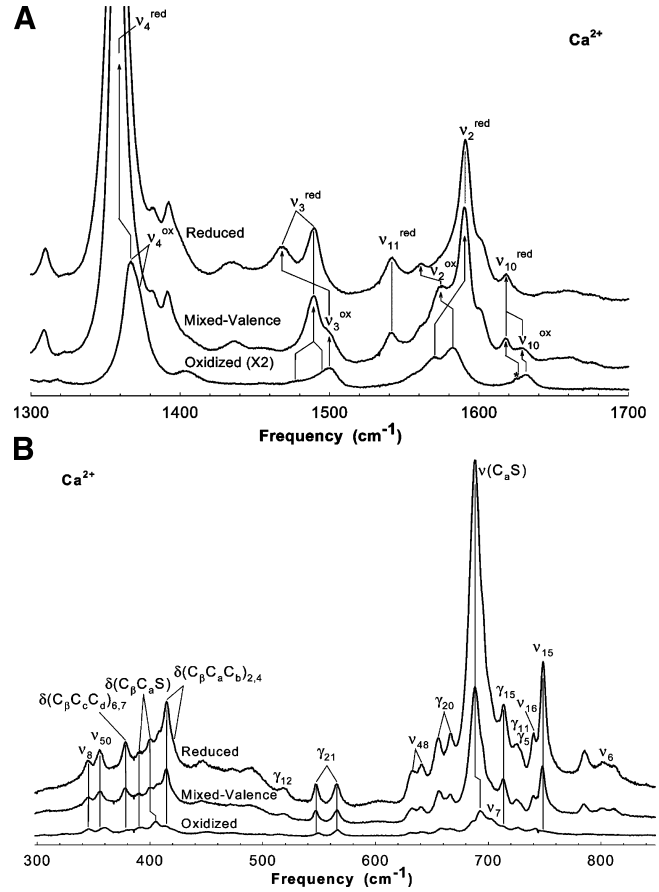

FIGURE 2: High-frequency (A) and low-frequency (B) resonance Raman spectra of 50 μM *P. pantotrophus* BCCP in 10 mM Hepes (pH 7.5) with added 2 mM calcium chloride. Spectra were recorded in the oxidized state by adding sodium ferricyanide, in the mixed-valence form by adding ascorbate and DAD, and in the fully reduced form by adding sodium dithionite. The asterisk denotes that an artifact caused by a laser emission line has been removed.

sensitive to oxidation, spin state, and macrocycle out-of-plane distortion (*16–19*), and when oxidation, coordination, and spin states are the same, the marker lines are particularly sensitive to nonplanar distortions (*20–26*), especially the ruffling-type deformation (*27, 28*).

Furthermore, asymmetry introduced by the macrocycle substituents and the out-of-plane and in-plane macrocycle distortion activates many other in-plane modes, out-of-plane modes, and substituent modes of other symmetries, with the out-of-plane vibrational modes being most evident in the low-frequency region (Figures 2B, 4, S1B, S2B, and S3B).

The RR spectra of both the mixed-valence and fully reduced forms of the enzyme in the low- and high-frequency regions (Figures 2 and S2) contain modes which are indicative of heme reduction and are sensitive to structural changes associated with Ca^{2+} concentrations. The sensitivity of the spectra to Ca^{2+} binding is specific since using NaCl to alter the ionic strength of the solution has an only small effect on the spectra of the EGTA-treated and as-isolated enzyme (Figures S3). This fact simplifies the analysis of the results because the principal changes observed are those due to calcium binding and not due to an increase in ionic strength. The minor changes that are observed with added NaCl, especially with the as-isolated sample, may result from the fact that the added NaCl promotes some dimerization

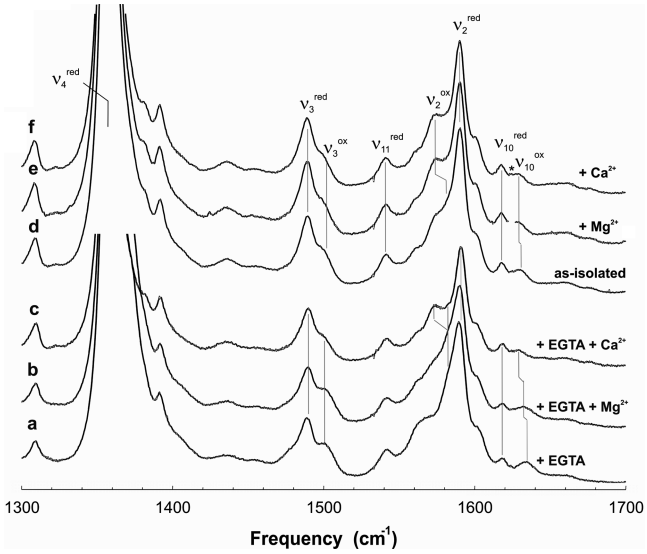

FIGURE 3: Resonance Raman spectra in the high-frequency region of 50 μM mixed-valence *Pa-p* BCCP under different conditions: (a) after pretreatment with 2 mM EGTA (+EGTA), (b) pretreated with EGTA, reduced ascorbate, and added 4 mM magnesium chloride (+EGTA+Mg^{2+}), (c) pretreated with EGTA, reduced ascorbate, and added 4 mM calcium chloride (+EGTA+Ca^{2+}), (d) as isolated, (e) as isolated, reduced ascorbate, and added 4 mM magnesium chloride (+Mg^{2+}), and (f) as isolated, reduced ascorbate, and added 4 mM calcium chloride (+Ca^{2+}). The asterisk denotes that an artifact caused by a laser emission line has been removed.

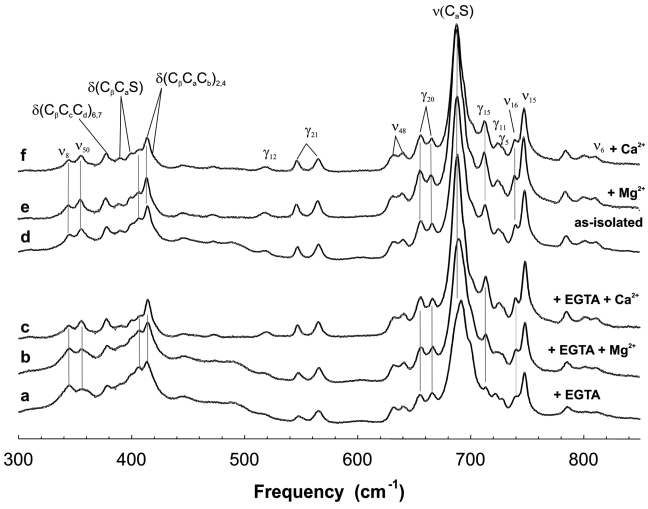

FIGURE 4: Resonance Raman spectra in the low-frequency region of 50 μM mixed-valence *Pa-p* BCCP under different conditions: (a) after pretreatment with 2 mM EGTA (+EGTA), (b) pretreated with EGTA, reduced ascorbate, and added 4 mM magnesium chloride (+EGTA+Mg^{2+}), (c) pretreated with EGTA, reduced ascorbate, and added 4 mM calcium chloride (+EGTA+Ca^{2+}), (d) as isolated, (e) as isolated, reduced ascorbate, and added 4 mM magnesium chloride (+Mg^{2+}), and (f) as isolated, reduced ascorbate, and added 4 mM calcium chloride (+Ca^{2+}).

and enhances binding of Ca^{2+} (*15*). The solutions contain an additional 6 mM NaCl as a control for the 2 mM divalent cations, and this may increase the amount of dimer, since it was previously shown that 50 mM NaCl promotes complete dimerization (*15*).

General Analysis of the High- and Low-Frequency RR Spectra. (i) High-Frequency In-Plane Vibrational Modes of the Heme. Figures 2A and S2A show the resonance Raman spectra of oxidized, mixed-valence, and fully reduced cytochrome *c* peroxidase in the high-frequency region with and without calcium at pH 7.5, respectively. The values of the line frequencies and normal mode assignments are listed in Tables S1 and S2 of the Supporting Information. The strong lines of the spectra in Figure 2A are mostly vibrations of A_{1g}, B_{1g}, and B_{2g} in-plane symmetries, but the polarized spectra reveal at least one A_{2g} mode [ν_{19}^{red}, near 1581 cm^{-1} (Figure S1)]. This line is apparently activated by heme reduction because it is not observed in the high-frequency region for the fully oxidized form of the *Pa-p* BCCP (*14*). The appearance of the ν_{19}^{red} line complicates the 1560−1600 cm^{-1} region, which is already subject to spectral crowding, but it is evident from the perpendicular polarized spectra in Figure S1 that the frequency and intensity of ν_{19}^{red} are practically Ca^{2+}-independent.

In the spectrum of the mixed-valence form, the intensities of the structure-sensitive marker lines (ν_2, ν_3, ν_4, and ν_{10}) of the oxidized peroxidatic heme are weaker than the lines of the reduced heme. Generally, the peak positions of these marker lines downshift upon reduction, but ν_2 is an exception. (This observation is verified by the comparison between the oxidized and fully reduced spectra of *Pa-p* BCCP, in Figures 2A and S2A.) In the Ca^{2+}-enriched mixed-valence enzyme, the ν_2 mode of the oxidized heme is assigned to the line at 1573 cm^{-1}, but it shifts to 1585 cm^{-1} on top of ν_{19}^{red}, for the same heme in the Ca^{2+}-depleted mixed-valence enzyme (see Figures 2A and S2A); the presence of ν_2 is most evident in the parallel polarized spectrum which would be expected for a polarized totally symmetric normal mode (Figure S1A). The 1603 cm^{-1} line is probably the E_u mode ν_{38} (or ν_{37}).

The frequencies of structure-sensitive marker lines ν_4, ν_3, ν_2, and ν_{10} of the RR spectrum of the mixed-valence enzyme, in the presence of calcium, are in good agreement with what is expected for an oxidized high-spin heme and a reduced low-spin heme, while in the calcium-depleted sample, the frequencies of these lines indicate that both the reduced and oxidized hemes are low-spin forms. Moreover, the frequencies of the marker lines in the high-frequency region of the RR spectra of the fully reduced peroxidase in the presence of calcium ions are indicative of one high-spin and one low-spin heme, while in the sample treated with EGTA, both hemes are low-spin.

(ii) Low-Frequency Skeletal and Substituent Vibrational Modes of the Heme. The assignments for Ca^{2+}-treated BCCP in three different oxidation states at pH 7.5 indicated in Figures 2B and S2B are based on the strong similarity between the frequencies and intensities and those of the corresponding Raman lines of yeast ferro- and ferricytochrome *c* isoenzyme-1 (*29*). The peak positions of the reduced forms are in agreement with what is expected for reduced low-spin hemes.

The intensities of the Raman lines vary with the oxidation state of the hemes, with the RR spectrum of fully oxidized BCCP being much weaker than that for the mixed-valence and fully reduced *Pa-p* BCCP spectra (Figures 2B and S2B). The 630−750 cm^{-1} region of the spectrum of the reduced hemes is especially strong. The RR spectrum of mixed-valence BCCP is very similar to the spectrum of fully reduced BCCP. One might expect to see lines indicative of both oxidized and reduced hemes in the spectrum of the mixed-valence form, but that is not the case. This could be due to several factors which include the intensities of the

oxidized heme peaks being relatively weak (Figures 2B and S2B), the high degree of congestion, and the lack of frequency shifts with spin-state and oxidation-state changes of lines in this region (*29*).

Effect of Different Cations on the Mixed-Valence Enzyme. Figures 3 and 4 show the effect of the addition of magnesium and calcium ions on the high- and low-frequency Raman spectra, respectively, of calcium-depleted and as-isolated mixed-valence *Pa-p* BCCP at pH 7.5. The frequencies of the lines and their normal mode assignments are listed in Tables S1 and S2.

From the previous study (*14*), we can divide the Raman spectra in Figures 3 and 4 into three categories: calcium-depleted (a, BCCP and EGTA; b, BCCP, EGTA, and Mg), partial calcium occupancy (d, as-isolated BCCP,), and calcium-enriched (c, BCCP, EGTA, and Ca; e, as-isolated BCCP and Mg; and f, BCCP and Ca). The spectrum of the EGTA-treated enzyme belongs to the calcium-depleted type, in which calcium is chelated out of the enzyme by EGTA. In contrast, the calcium-enriched type includes the spectra of BBCP for which the calcium sites are fully occupied by calcium ions, and in the remaining spectra, occupancy of calcium site 2 is incomplete.

(i) High-Frequency In-Plane Vibrational Modes of the Heme. The frequencies of structure-sensitive lines ν_2, ν_3, ν_4, and ν_{10} of *Paracoccus* BCCP are in good agreement with what is expected for one reduced low-spin heme and one oxidized high-spin or low-spin heme, depending on whether Ca^{2+} (or in some cases Mg^{2+}) is present in solution to cause the conversion to the high-spin form (Figure 3).

Since the reduced heme of the mixed-valence form is always in the low-spin configuration, the shifts of the structure-sensitive marker lines associated with this reduced heme among the three different protein types are relatively small and most likely are due only to heme structural changes caused by calcium binding. For the top three spectra in Figure 3 (d−f), the peak shapes and maximum frequencies associated with the reduced heme are very similar. However, when these spectra are compared with the EGTA-treated ones (Figure 3, spectra a−c), we do observe small but significant peak frequency shifts. For example, ν_2^{red} is downshifted from 1590.6 to 1590.0 cm^{-1} for the spectrum of BCCP and EGTA. This reveals that the filling of the calcium site with calcium ions only weakly affects the structure of the reduced electron-transferring heme.

For the oxidized heme of the mixed-valence protein, the Ca^{2+}-dependent changes of the structure-sensitive marker lines are considerably larger than for the reduced heme. For example, ν_{10}^{ox} of the calcium-depleted-type spectrum (BCCP and EGTA) is at 1635 cm^{-1}, that of the as-isolated-type spectra at 1631 cm^{-1}, and that of the calcium-enriched-type spectrum (BCCP and Ca) at 1629 cm^{-1}. More importantly, ν_2 of the oxidized heme is resolved at 1573 cm^{-1} for the Ca^{2+}-enriched protein spectrum, consistent with other five-coordinate high-spin proteins (*30*), but this line virtually disappears for the other spectra. Thus again, we see that it is the oxidized heme of the mixed-valence form that exhibits the largest Ca^{2+}-dependent changes. Subtle changes in the relative intensity of the lines from the oxidized and reduced hemes are also noticed in Figure 3; for example, notice the ratio of the intensities of the ν_{10} lines of the oxidized and reduced hemes. Such intensity differences are not a result of differences in the amount of reduction, but rather due to differences in the resonance Raman enhancements of the hemes altered by cation binding, given that all mixed-valence protein samples have the electron-transferring heme fully reduced and the peroxidatic heme oxidized.

The influence of calcium binding on the heme conformation was further examined by another series of RR experiments on samples that were pretreated with EGTA to completely remove the Ca^{2+} (Figure 3). Previous spectroscopic studies suggested that, although magnesium ions could bind to the as-isolated enzyme and activate it, magnesium ion could not bind to the enzyme after EGTA treatment. This led to the proposal of two calcium-binding sites (site 1 and site 2) with the latter being responsible for enzyme activation and the former being occupied by calcium ion in the as-isolated state [and not detectable in the X-ray structure (*12*)]. Occupancy of site 1 is required for binding to site 2, but magnesium ion cannot occupy site 1 (*31*).

To examine this hypothesis, magnesium and calcium ions were added to the Ca^{2+}-depleted solutions, and the results are shown in Figure 3. When Mg^{2+} was added to the solution, some small spectral changes were observed, but the ν_2^{ox} line, which is characteristic of full occupancy of calcium site 2 (see Figure 3f), appeared only after addition of Ca^{2+}, producing a spectrum essentially the same as the spectrum obtained for addition of Ca^{2+} to the as-isolated protein. This suggests that only Ca^{2+} can produce the expected spectral changes, in agreement with previous suggestions that Mg^{2+} cannot occupy site 1. When calcium ions were added back into the solution completely filling both binding sites, spectrum c (BCCP, EGTA, and Ca) shown in Figure 3 is essentially the same as the spectrum of the as-isolated protein with added calcium shown in Figure 3f (BCCP and Ca).

(ii) Low-Frequency Skeletal and Substituent Vibrational Modes of the Heme. Figure 4 shows RR spectra of mixed-valence BCCP in the low-frequency region at pH 7.5 with and without EGTA pretreatment. Lines in the 300−850 cm^{-1} region that show calcium-dependent changes are assigned to in-plane and out-of-plane macrocycle modes as well as modes associated with the substituents (Tables S1 and S2). Close inspection of the spectra in Figure 4 reveals that the top three spectra are very similar but different from the EGTA-treated BCCP spectrum at the bottom. When the protein is entirely depleted of Ca^{2+} (Figure 4a, BCCP and EGTA), significant changes are observed; in particular, $\nu(C_aS)$ is upshifted and the intensity of γ_{15} is reduced considerably. Although, without EGTA pretreatment, the spectrum with added Mg^{2+} is very much like that of the protein with added Ca^{2+}, the addition of Mg^{2+} to the EGTA-pretreated protein gives a spectrum (Figure 4b) that is more like the spectrum of the EGTA-treated protein (Figure 4a), with very few changes been observed in the intensity of some modes.

It is important to point out that, because of the increased intensity of the spectra of the reduced form, it might seem that the ferrous electron-transferring heme of the mixed-valence protein is the main contributor to the low-frequency region of the Raman spectra. If this were the case, then most of the Ca^{2+}-dependent spectral changes in Figure 4 would have to result from the small structural changes in the ferrous electron-transferring heme detected in the structure-sensitive lines in the high-frequency region. Nevertheless, there

remains the remote possibility that at least some of these spectral changes come from the ferric peroxidatic heme. The reason is that the large Ca^{2+}-dependent structural changes in the ferric peroxidatic heme could result in a sufficiently large increase in the intensity of its spectrum for some of its lines to contribute strongly in Figure 4. The Ca^{2+}-dependent spectral changes in the low-frequency region are evident even with calcium site 2 partially filled; significant differences in the modes of the covalent linkage of the heme to the protein and in the structure-sensitive and out-of-plane modes are observed. In particular, an intensity ratio reversal for ν_8 and ν_{50} and changes in the substituent modes associated with the thioether linkages and prominent out-of-plane modes of B_{1u}, B_{2u}, and E_g symmetries are observed.

DISCUSSION

The mixed-valence form of *P. pantotrophus* cytochrome *c* peroxidase must be in the dimeric state with bound calcium ions at site 2 to be active. Calcium site 2 is located between the electron-transferring and peroxidatic heme, at the domain interface, based on the crystal structure of this enzyme (*12*). Although there is much spectroscopic evidence of the presence of a putative calcium site 1, this site has not been detected by crystallography. Even though Ca^{2+} binding site 2 is not sufficiently close to be in direct contact with the hemes, the heme conformation can be altered indirectly by changes in the protein structure induced by Ca^{2+} binding (*12, 14*). For the inactive oxidized form of BCCP, the previous RR study showed that calcium binding to the empty sites (Figure 1, form a) induces distortion of the peroxidatic heme but not much change in the electron-transferring heme (*14*). Further, the change in the out-of-plane distortion of the peroxidatic heme is coincident with Ca^{2+}-induced conformational changes in the heme-linked fingerprint peptide. In fact, the change in heme distortion may result from alteration of the covalent linkages to the peroxidatic heme. For the oxidized enzyme, these structural changes do not lead to an active protein with an open coordination site for peroxide (*14*).

To determine the influence of the binding of calcium ions on the structure of the hemes of the active mixed-valence protein, the mixed-valence form was investigated after incubation under different solution conditions. The conditions assayed at pH 7.5 in this study were as follows: (1) empty calcium sites (BCCP and EGTA; BCCP, EGTA, and Mg), (2) partial occupancy [as-isolated BCCP (Figure 1, form b)], and (3) full occupancy of the sites [BCCP, EGTA, and Ca; as-isolated BCCP and Ca; as-isolated BCCP and Mg (Figure 1, form c)].

Effects of Heme Oxidation State. For the fully oxidized enzyme, the RR spectra of both hemes are generally weak (Figures 2 and S2), when compared with the RR spectra of both the mixed-valence and fully reduced enzyme. In the case of the fully oxidized BCCP with Ca^{2+}, the frequency of the marker lines, in the high-frequency region (Figure 2A), is consistent with the presence of a bis-histidine low-spin and a six-coordinate partially high-spin ferric heme, which can be assigned to the peroxidatic and electron-transferring heme, respectively (*14*). For the oxidized protein, in the absence of Ca^{2+} (Figure S2A), the high-spin lines are even weaker, and the only manifestation of the partially high-spin heme in the spectrum of the oxidized EGTA-treated protein is in the line shape of ν_4, which exhibits a clear shoulder on the low-frequency side (Figure S1A) at 1368 cm^{-1}. [With added Ca^{2+}, the intensities of the two ν_4 lines invert (Figure S1A).]

As mentioned, the mixed-valence proteins show strong overall increases in intensity of the high-frequency Raman marker lines compared to the oxidized protein, with the lines of the reduced electron-transferring heme dominating the spectrum (Figures 2A and S2A). For the mixed-valence enzyme in the presence of added Ca^{2+}, the strong marker lines of the reduced electron-transferring heme (Tables S1 and S2 and Figure 2A) are consistent with a ferrous low-spin His-Met-coordinated heme *c*. Although the frequencies of all the lines are 5−8 cm^{-1} low compared to those of yeast isozyme-1 cytochrome *c* (*29*), they are in much better agreement with frequencies of the marker lines for the horse ferrocytochrome *c* [which are at 1360 (ν_4), 1490 (ν_3), 1590 (ν_2), and 1619 cm^{-1} (ν_{10}) (spectrum not shown)]. However, the lines of ferrocytochrome c_3 (which has bis-histidine coordination) are close to these frequencies; thus, it is impossible to distinguish His/Met and His/His coordination on the basis of the frequencies of the structure-sensitive Raman lines alone.

In the case of the mixed-valence BCCP, there are large differences evident in the RR spectra of the ferric peroxidatic heme resulting from the protein structural changes associated with reduction of the electron-transferring heme and Ca^{2+} binding. The spectral changes in the weaker lines of the ferric peroxidatic heme are clearly observed because of the large frequency shifts associated with reduction of the electron-transferring heme. The ν_3, ν_2, and ν_{10} lines of the ferric peroxidatic heme shift from 1501, 1583, and 1633 cm^{-1} for the oxidized protein to 1500, 1573, and 1630 cm^{-1}, respectively (Table S1), for the calcium-enriched mixed-valence protein (Figure 1, form d). ν_2 shows the largest shift, a decrease of 10 cm^{-1} upon reduction of the electron-transferring heme. These shifts of the ferric peroxidatic heme are due to the combined effects of the change from low-spin to high-spin and the loss of one of the histidine axial ligands, which occurs in the presence of excess Ca^{2+}. The heme of freshly prepared yeast cytochrome *c* peroxidase is also pentacoordinate high-spin and has the corresponding marker lines at 1494, 1570, and 1628 cm^{-1} (*30*).

For the calcium-depleted mixed-valence protein, the changes in the RR spectrum of the ferric peroxidatic heme upon reduction of the electron-transferring heme (Figure S2) are similar to that illustrated in Figure 2 for the calcium-treated protein. However, the frequencies of marker lines ν_3 (1501 cm^{-1}), ν_2 (1573 cm^{-1}), and ν_{10} (1630 cm^{-1}) change by 1, 12, and 5 cm^{-1}, respectively, relative to the calcium-enriched enzyme and are indicative of hexacoordinate low-spin ferric heme as in yeast cytochrome *c* (*14, 29*). Thus, the RR results confirm the proposed changes from a low-spin hexacoordinate heme to a catalytically active high-spin pentacoordinate heme upon Ca^{2+} binding (Figure 1, form d).

Fully Reduced BCCP. For the fully reduced protein, the marker line frequencies of the two hemes are apparently so similar that individual lines cannot be resolved, except for ν_3. In Figure 2 (added Ca^{2+}), the main effect of reduction of the second heme is the disappearance of the lines of the oxidized heme and the appearance of a ν_3 line at 1468 cm^{-1},

which suggests a pentacoordinate high-spin ferrous heme. Along with the ν_3 line, there is a weak line at 1562 cm^{-1} in the spectrum of the Ca^{2+}-treated fully reduced protein (Figure 2) that may contain a ν_2 contribution from a pentacoordinate high-spin heme, when comparing the frequencies of these marker lines with the ones of ferrous yeast BCCP, which contains a pentacoordinate high-spin heme (*30*). Furthermore, the lack of a qualitative increase in the intensities of ν_3 and ν_2 of the low-spin ferrous hexacoordinate form at 1489 and 1591 cm^{-1}, respectively, when the second heme is reduced (and Ca^{2+} is present) also supports the formation of a pentacoordinate ferrous species.

On the other hand, when both the reduced peroxidatic heme and the reduced electron-transferring heme are low-spin hexacoordinate forms [EGTA-treated fully reduced spectrum (Figure S2A)], these lines do approximately double in intensity when compared with those of the mixed-valence form. Thus, the Raman data are consistent with the model in which Ca^{2+} binding removes the sixth ligand of the peroxidatic heme and changes it to a high-spin pentacoordinate type in the mixed-valence form, and the peroxidatic heme remains pentacoordinate even when it is reduced.

The effects of heme reduction are also observed in the low-frequency region of the RR spectra (Figures 2B and S2B). Strong overall increases in the intensity of the RR spectrum and clear differences in the relative intensities of the lines are observed. In particular, the appearance of strong ν_{15} and γ_{15} modes of the heme macrocycle suggests changes in the macrocyclic distortion. The appearance of γ_{15} is not due to reduction by itself because its enhancement is calcium-dependent (vide infra).

Large changes in the substituent-dependent modes also occur upon reduction; most noteworthy are the changes in the vinyl linkage modes [$\delta(C_\beta C_c C_d)_{6,7}$]. Because of the large increase in intensity of the lines of the reduced heme, it is likely that many of the spectral differences are associated with reduction of the heme rather than the differences in the structure of the oxidized peroxidatic heme. Specifically, the increased intensity in the propionate modes [$\delta(C_\beta C_c C_d)_{6,7}$] of the mixed-valence enzyme, in the presence of Ca^{2+} and to a lesser extent Mg^{2+}, can be attributed to the electron-transferring heme, since it was observed that the orientation of the D propionate group of this heme changes upon reduction, in the presence of calcium ions (*12*). In fact, Pettigrew et al. have suggested that in the presence of calcium ions, there is a redox-couple Bohr effect occurring at this heme that triggers the structural rearrangements which in turn enables the loss of the sixth ligand at the peroxidatic heme (*32*). The RR results obtained corroborate this hypothesis, since this mode becomes more prominent only when calcium site 2 is being filled.

The contribution of the oxidized heme to the spectrum of the mixed-valence protein, in Figure 2B, is unclear, and this is underscored by the fact that most of the RR lines exhibit a further increase in intensity when the peroxidatic heme is also reduced. Other than the increased intensity, there is not much difference between the spectra of the mixed-valence and fully reduced proteins.

Effect of Calcium Binding on the Ferrous Electron-Transferring Heme of Mixed-Valence BCCP. For the mixed-valence protein, the reduced electron-transferring heme, as for the fully oxidized protein (*14*), exhibits minimal changes in the nonplanarity of the heme macrocycle with filling of calcium sites, as indicated by the small differences in the frequencies of the structure-sensitive lines for the as-isolated and EGTA-treated proteins. For example, ν_{10}^{red} and ν_2^{red} are downshifted 0.6 cm^{-1} and upshifted 0.8 cm^{-1}, respectively, for as-isolated protein relative to the EGTA-treated protein (Figure 3; but too small to be apparent on this scale), and the complete filling of the calcium sites has little further effect on the electron-transferring heme conformation (Figure 3). In addition, the frequency shifts are not of a recognizable pattern associated with a particular type of deformation with a change in axial ligands since ν_2^{red} and ν_{10}^{red} change in the opposite senses. Both ν_{10} and ν_2 lines are ruffling-sensitive, but ν_2 also shifts due to changes in the peripheral substituents, which may account for its shift in the opposite direction. This could mean that the reduced electron-transferring heme becomes a little more ruffled when calcium ions completely fill the sites in the mixed-valence form, but for such small frequency shifts, other types of nonplanar deformation cannot be ruled out (*33*).

The low-frequency RR results for the electron-transferring heme (Figure 4) provide little information because it is not clear which heme contributes most to the spectra. However, as discussed above, the increased intensity of the propionate modes [$\delta(C_\beta C_c C_d)_{6,7}$] upon reduction and occupancy of the calcium sites can be attributed to this heme. The other Ca^{2+}-dependent spectral changes observed in this region might be attributed to changes in the peroxidatic heme (vide infra).

Effect of Calcium Binding on the Ferric Peroxidatic Heme of Mixed-Valence BCCP. Upon reduction of electron-transferring heme, with calcium site 2 completely filled, the peroxidatic heme loses its sixth ligand and becomes available to bind the substrate; therefore, one does expect substantial structural changes in the ferric peroxidatic heme to occur. In our previous study of fully oxidized *Paracoccus* BCCP (*14*), the RR spectra in the low-frequency region showed that the Ca^{2+} changes were consistent with an increase in the out-of-plane distortion of the peroxidatic heme caused by a structural change in the covalently linked pentapeptide (CQTCH). The Ca^{2+}-dependent changes in the mixed-valence form of the enzyme now further support the conclusion that Ca^{2+}-dependent structural changes can be attributed to the peroxidatic heme.

The Raman data support relatively large structural changes in the ferric peroxidatic heme of the mixed-valence protein when calcium site 2 is filled. For example, the downshift for ν_{10}^{ox} as the site is filled is 4.0 cm^{-1} (EGTA-treated minus as-isolated). An additional downshift in ν_{10}^{ox} of 1.0 cm^{-1} occurs when site 2 is completely filled along with the change in both spin and coordination states.

Similar but larger changes are observed for ν_2^{ox}. Curve fitting gives this line at 1585 cm^{-1} for the EGTA-treated protein, as expected for low-spin six-coordinate heme, which becomes stronger and fully resolved when Ca^{2+} is added. These Ca^{2+}-dependent changes are completely consistent with the RR frequencies of marker lines for a ferric low-spin heme with two histidine ligands, which undergoes significant structural changes upon filling of calcium site 2 and converts to a five-coordinate high-spin form.

The shoulder at 1573 cm^{-1} (Figure 3, as-isolated spectrum) may be ν_2^{ox}, indicating the presence of some five-coordinate high-spin heme with partial filling of calcium site 2.

However, it is clear from the much-increased intensity of this line after Ca^{2+} is added (Figure 3) that complete conversion to the five-coordinate high-spin ferric heme occurs only when calcium site 2 is completely filled. The loss of the sixth histidine ligand and opening of a free axial coordination site facilitate reactivity of BCCP with hydroperoxides because sixth ligand dissociation is likely rate-limiting (*34*). This view is also in agreement with the recent crystal structure of the BCCP from *P. pantotrophus* in the mixed-valence form, which shows the heme in a pentacoordinate form with histidine as the only axial ligand (*12*).

Ca^{2+}-Dependent Changes in the Conformation and Substituents of the Ferric Peroxidatic Heme. As mentioned in Results, we are faced with ambiguity in determining which heme is responsible for the significant differences in the low-frequency RR spectra of the mixed-valence protein observed under various solution conditions (Figure 4). It is tempting to ascribe at least some of these calcium-dependent changes to the peroxidatic heme, since this heme shows the major Ca^{2+}-dependent changes in macrocycle and substituent conformations for the fully oxidized protein (*14*). In addition, the high-frequency structure-sensitive lines of the ferric peroxidatic heme of the mixed-valence protein indicate that changes in conformation occur. Moreover, changes should be observable in the low-frequency region if the heme distortion brings about suitable enhancement of the RR lines of the ferric peroxidatic heme.

The calcium-dependent changes in the heme substituent modes indicate significant changes, especially in the thioether linkages to the protein. In particular, the C_aS stretching modes are at 688 and 692 cm^{-1} for the mixed-valence protein. [The $\nu(C_aS)$ modes are assigned by comparison with ferrocytochrome *c*, which has these lines at 682 and 692 cm^{-1}; these lines coalesce for ferricytochrome *c* into a single line at 693 cm^{-1}.] The relative intensities of these two lines depend strongly on the binding of Ca^{2+}, both for the oxidized and for the mixed-valence forms. When Ca^{2+} is present, the low-frequency line is greatly enhanced for the mixed-valence form, almost obscuring the high-frequency $\nu(C_aS)$ line, but when Ca^{2+} is absent, the high-frequency $\nu(C_aS)$ line is more enhanced. This appears to give a shift from 692 to 688 cm^{-1} as calcium site 2 is filled (Figure 4), which shows clearly that the cysteine linkages to the peroxidatic heme (oxidized) are appreciably altered by complete filling of calcium sites. Similarly, the other regions associated with the cysteine linkages to the hemes are influenced by Ca^{2+} binding to the protein, especially the bending motions of the sulfur [$\delta(C_\beta C_aS)$] (downshifts 1 cm^{-1}) and other motions of the 2- and 4-linkages to the protein [$\delta(C_\beta C_a C_b)_{2,4}$] (upshifts 1 cm^{-1}). In contrast, the propionate bending modes [$\delta(C_\beta C_c C_d)_{6,7}$] present a smaller change upon binding of calcium ions to the enzyme (Figure 4), and as mentioned before, these modes can be attributed to the electron-transferring heme.

The conformation of the peroxidatic heme macrocycle of the mixed-valence form is appreciably altered when calcium site 2 is partially filled. This conformational change is indicated by changes in the low-frequency skeletal modes of the porphyrin as well as the out-of-plane modes. For example, ν_8 and ν_{50} are related in-plane modes of the macrocycle and are known to be sensitive to out-of-plane distortion of the heme, especially to ruffling of the macrocycle. It is seen in Figure 4 that the relative intensities, line shape, and frequencies of these two modes are especially sensitive to the fractional filling of calcium site 2, with ν_{50} downshifting by 2 cm^{-1}.

Several of the out-of-plane modes are also Ca^{2+}-dependent. For example, γ_{12}, a B_{1u}-symmetry (ruffling-type) mode, appears more prominently in the proteins which are partially filled with calcium ion (Figure 4). Similarly, the Ca^{2+}-dependent changes in E_g modes γ_{20} and γ_{21}, which show shifts of 1 cm^{-1}, indicate an alteration in the wavelike deformations of the macrocycle also upon fractional occupation of calcium site 2.

One of the most striking changes upon partial filling of calcium site 2 is the appearance of a moderately strong B_{2u} saddling-type mode that is assigned to γ_{15} at 713 cm^{-1} (Figure 4). This mode appears prominently in almost all peroxidases (G. Smulevich, personal communication). Significantly, almost all peroxidases are also known to have predominantly saddled hemes in their X-ray crystal structures (*28*), and the appearance of a strong γ_{15} line for the mixed-valence *Paracoccus* enzyme might be expected if the peroxidatic heme becomes more saddled (like other peroxidases) during the conformational changes that activate the enzyme. This line most certainly does not appear just because of reduction of the electron-transferring heme, as it is not prominent in the spectra of the mixed-valence or fully reduced protein in the absence of Ca^{2+} (Figure S2B). Its enhancement is clearly associated with occupation of calcium sites.

Ascribing these low-frequency spectral changes, particularly the increased intensity of γ_{15}, to Ca^{2+}-dependent structural changes of the peroxidatic heme is further supported by the lack of significant shifts in the high-frequency lines of the ferrous electron-transferring heme known to be sensitive to both saddling and ruffling (*33*). Furthermore, the spectral changes that occur in the low-frequency region of the mixed-valence protein are very similar to those that occur for the peroxidatic heme of the fully oxidized protein. That is, calcium-dependent changes in B_{1u}, B_{2u}, and E_g types of deformation are evident in the low-frequency spectra of the mixed-valence form, just as they are for the fully oxidized protein. We conclude that the lack of shifts in the high-frequency marker lines of the reduced heme suggests that at least some of the changes in the low-frequency out-of-plane modes are due to the oxidized peroxidatic heme. These vibrational modes experience a gain in overall intensity because of the loss of the sixth ligand and/or enhancement caused by out-of-plane distortion. Apparently, this structural influence of complete binding of calcium to the mixed-valence protein is required for the conformational conversion of the heme that results in enzymatic activity.

Effect of Mg^{2+} Binding to the Mixed-Valence BCCP. The addition of Mg^{2+} to the as-isolated mixed-valence enzyme seems to involve the same changes as the addition of Ca^{2+}, suggesting that magnesium ion can occupy site 2 in place of calcium ion. However, when magnesium ions are added to the calcium-depleted enzyme (Figures 3 and 4), the intensities of high-frequency modes ν_3^{ox}, ν_2^{ox}, and ν_{10}^{ox} are not the same as those that are achieved with addition of calcium ion, which would mean that the peroxidatic heme is not completely five-coordinate. In the low-frequency region, there are even more modes that do not present the

same shift or intensity as in the enzyme with the calcium sites fully occupied. The out-of-plane macrocycle modes and heme substituents, including the γ_{15} saddling-symmetry mode, as well as ν_8 and ν_{50} do not present the same intensity when calcium or magnesium ions are added. This is consistent with the previous proposal that magnesium ions can enter site 2 but not site 1 and that occupancy of site 1 is required for entry to site 2.

CONCLUSIONS

The resonance Raman data provide detailed information concerning the heme conformational changes that are calcium-dependent and that lead to activation in conjunction with the coordination and spin-state changes. In particular, the binding of calcium ion to the mixed-valence protein appears to introduce a significant saddling and other types of distortion of one of the hemes, most likely the peroxidatic ferric heme, in concurrence with all other peroxidase crystal structures of the active enzymes.

The RR spectra also support the current view of the spin-, coordination-, and oxidation-state changes that bring about the peroxidase activity of the mixed-valence form of the enzyme, in that the enzyme is only fully pentacoordinate and activated when calcium site 2 is completely filled with calcium ions. The results obtained corroborate the hypothesis that the proposed trigger for the structural rearrangement, which is associated with the reduction of the electron-transferring heme and a change in the orientation of the D propionate group, requires the occupancy of the calcium sites.

Moreover, the resonance Raman spectra show for the first time that in the fully reduced state the peroxidatic heme remains in a high-spin configuration.

SUPPORTING INFORMATION AVAILABLE

Tables S1 and S2 list the frequencies of the Raman lines of various forms of the mixed-valence enzyme. Figure S1 shows the polarized resonance Raman spectra of the mixed-valence form with added calcium ions or pretreated with EGTA. Figure S2 shows the RR spectra of fully reduced, mixed-valence, and oxidized BCCP pretreated with EGTA. Figure S3 showing the effect of Na^+ on the resonance Raman spectra of mixed-valence *Pa-p* BCCP pretreated with EGTA or in the as-isolated form. This material is available free of charge via the Internet at http://pubs.acs.org.

REFERENCES

1. Lesser, M. P. (2006) Oxidative stress in marine environments: Biochemistry and physiological ecology. *Annu. Rev. Physiol. 68*, 253–278.
2. Soininen, R., and Ellfolk, N. (1972) *Pseudomonas* cytochrome *c* peroxidase. 4. Some kinetic properties of peroxidation reaction, and enzymatic determination of extinction coefficients of *Pseudomonas* cytochrome *c*-551 and azurin. *Acta Chem. Scand. 26*, 861–872.
3. Pauleta, S. R., Guerlesquin, F., Goodhew, C. F., Devreese, B., Van Beeumen, J., Pereira, A. S., Moura, I., and Pettigrew, G. W. (2004) *Paracoccus pantotrophus* pseudoazurin is an electron donor to cytochrome *c* peroxidase. *Biochemistry 43*, 11214–11225.
4. Ronnberg, M., and Ellfolk, N. (1979) Heme-linked properties of *Pseudomonas* cytochrome *c* peroxidase: Evidence for nonequivalence of the hemes. *Biochim. Biophys. Acta 581*, 325–333.
5. Hanlon, S. P., Holt, R. A., and Mcewan, A. G. (1992) The 44 kDa *c*-type cytochrome induced in *Rhodobacter capsulatus* during growth with dimethylsulfoxide as an electron-acceptor is a cytochrome-*c* peroxidase. *FEMS Microbiol. Lett. 97*, 283–288.
6. Hu, W., De Smet, L., Van Driessche, G., Bartsch, R. G., Meyer, T. E., Cusanovich, M. A., and Van Beeumen, J. (1998) Characterization of cytochrome *c*-556 from the purple phototrophic bacterium *Rhodobacter capsulatus* as a cytochrome *c* peroxidase. *Eur. J. Biochem. 258*, 29–36.
7. Arciero, D. M., and Hooper, A. B. (1994) A di-heme cytochrome *c* peroxidase from *Nitrosomonas europaea* catalytically active in both the oxidized and half-reduced states. *J. Biol. Chem. 269*, 11878–11886.
8. Alves, T., Besson, S., Duarte, L. C., Pettigrew, G. W., Girio, F. M. F., Devreese, B., Vandenberghe, I., Van Beeumen, J., Fauque, G., and Moura, I. (1999) A cytochrome *c* peroxidase from *Pseudomonas nautica* 617 active at high ionic strength: Expression, purification and characterization. *Biochim. Biophys. Acta 1434*, 248–259.
9. Timoteo, C. G., Tavares, P., Goodhew, C. F., Duarte, L. C., Jumel, K., Girio, F. M. F., Harding, S., Pettigrew, G. W., and Moura, I. (2003) Ca^{2+} and the bacterial peroxidases: The cytochrome *c* peroxidase from *Pseudomonas stutzeri*. *J. Biol. Inorg. Chem. 8*, 29–37.
10. Zahn, J. A., Arciero, D. M., Hooper, A. B., Coats, J. R., and DiSpirito, A. A. (1997) Cytochrome *c* peroxidase from *Methylococcus capsulatus* Bath. *Arch. Microbiol. 168*, 362–372.
11. Goodhew, C. F., Wilson, I. B. H., Hunter, D. J. B., and Pettigrew, G. W. (1990) The cellular location and specificity of bacterial cytochrome *c* peroxidases. *Biochem. J. 271*, 707–712.
12. Echalier, A., Goodhew, C. F., Pettigrew, G. W., and Fulop, V. (2006) Activation and catalysis of the di-heme cytochrome *c* peroxidase from *Paracoccus pantotrophus*. *Structure 14*, 107–117.
13. Gilmour, R., Goodhew, C. F., Pettigrew, G. W., Prazeres, S., Moura, I., and Moura, J. J. G. (1993) Spectroscopic characterization of cytochrome *c* peroxidase from *Paracoccus denitrificans*. *Biochem. J. 294*, 745–752.
14. Pauleta, S. R., Lu, Y., Goodhew, C. F., Moura, I., Pettigrew, G. W., and Shelnutt, J. A. (2001) Calcium-dependent conformation of a heme and fingerprint peptide of the diheme cytochrome *c* peroxidase from *Paracoccus pantotrophus*. *Biochemistry 40*, 6570–6579.
15. Pettigrew, G. W., Goodhew, C. F., Cooper, A., Nutley, M., Jumel, K., and Harding, S. E. (2003) The electron transfer complexes of cytochrome *c* peroxidase from *Paracoccus denitrificans*. *Biochemistry 42*, 2046–2055.
16. Yamamoto, T., Palmer, G., FGill, D., Salmeen, I. T., and Lajos, R. (1973) The valence and spin state of iron in oxyhemoglobin as inferred from resonance Raman spectroscopy. *J. Biol. Chem. 248*, 5211–5213.
17. Spiro, T. G., and Strekas, T. C. (1974) Resonance Raman spectra of heme proteins. Effects of oxidation and spin state. *J. Am. Chem. Soc. 96*, 338–345.
18. Spiro, T. G., and Burke, J. M. (1976) Protein control of porphyrin conformation. Comparison of resonance Raman spectra of heme proteins with mesoporphyrin IX analogues. *J. Am. Chem. Soc. 98*, 5482–5489.
19. Spiro, T. G. (1982) in *Iron Porphyrins* (Lever, A. B. P., and Gray, H. B., Eds.) pp 89, Addison-Wesley, Reading, MA.
20. Alden, R. G., Crawford, B. A., Doolen, R., Ondrias, M. R., and Shelnutt, J. A. (1989) Ruffling of nickel(II) octaethylporphyrin in solution. *J. Am. Chem. Soc. 111*, 2070–2072.
21. Li, X. Y., Czernuszewicz, R. S., Kincaid, J. R., and Spiro, T. G. (1989) Consistent porphyrin force-field. 3. Out-of-plane modes in the resonance Raman-spectra of planar and ruffled nickel octaethylporphyrin. *J. Am. Chem. Soc. 111*, 7012–7023.
22. Shelnutt, J. A., Medforth, C. J., Berber, M. D., Barkigia, K. M., and Smith, K. M. (1991) Relationships between structural parameters and Raman frequencies for some planar and nonplanar nickel(II) porphyrins. *J. Am. Chem. Soc. 113*, 4077–4087.
23. Shelnutt, J. A., Majumder, S. A., Sparks, L. D., Hobbs, J. D., Medforth, C. J., Senge, M. O., Smith, K. M., Miura, M., Luo, L., and Quirke, J. M. E. (1992) Resonance Raman spectroscopy of nonplanar nickel porphyrins. *J. Raman Spectrosc. 23*, 523–529.
24. Song, X. Z., Jentzen, W., Jaquinod, L., Khoury, R. G., Medforth, C. J., Jia, S. L., Ma, J. G., Smith, K. M., and Shelnutt, J. A. (1998) Substituent-induced perturbation symmetries and distortions of meso-tert-butylporphyrins. *Inorg. Chem. 37*, 2117–2128.
25. Jentzen, W., Simpson, M. C., Hobbs, J. D., Song, X., Ema, T., Nelson, N. Y., Medforth, C. J., Smith, K. M., Veyrat, M., Mazzanti, M., Ramasseul, R., Marchon, J. C., Takeuchi, T., Goddard, W. A., and Shelnutt, J. A. (1995) Ruffling in a series of nickel(II) meso-

tetrasubstituted porphyrins as a model for the conserved ruffling of the heme of cytochromes *c*. *J. Am. Chem. Soc. 117*, 11085–11097.
26. Shelnutt, J. A., Song, X. Z., Ma, J. G., Jia, S. L., Jentzen, W., and Medforth, C. J. (1998) Nonplanar porphyrins and their significance in proteins. *Chem. Soc. Rev. 27*, 31–41.
27. Ma, J. G., Zhang, J., Franco, R., Jia, S. L., Moura, I., Moura, J. J. G., Kroneck, P. M. H., and Shelnutt, J. A. (1998) The structural origin of nonplanar heme distortions in tetraheme ferricytochromes c_3. *Biochemistry 37*, 12431–12442.
28. Howes, B. D., Schiodt, C. B., Welinder, K. G., Marzocchi, M. P., Ma, J. G., Zhang, J., Shelnutt, J. A., and Smulevich, G. (1999) The quantum mixed-spin heme stale of barley peroxidase: A paradigm for class III peroxidases. *Biophys. J. 77*, 478–492.
29. Hu, S. Z., Morris, I. K., Singh, J. P., Smith, K. M., and Spiro, T. G. (1993) Complete assignment of cytochrome *c* resonance Raman spectra via enzymatic reconstitution with isotopically labeled hemes. *J. Am. Chem. Soc. 115*, 12446–12458.
30. Dasgupta, S., Rousseau, D. L., Anni, H., and Yonetani, T. (1989) Structural characterization of cytochrome *c* peroxidase by resonance Raman scattering. *J. Biol. Chem. 264*, 654–662.
31. Gilmour, R., Prazeres, S., McGinnity, D. F., Goodhew, C. F., Moura, J. J. G., Moura, I., and Pettigrew, G. W. (1995) The affinity and specificity of Ca^{2+} binding sites of cytochrome *c* peroxidase from *Paracoccus denitrificans*. *Eur. J. Biochem. 234*, 878–886.
32. Pettigrew, G. W., Echalier, A., and Pauleta, S. R. (2006) Structure and mechanism in the bacterial dihaem cytochrome *c* peroxidases. *J. Inorg. Biochem. 100*, 551–567.
33. Franco, R., Ma, J. G., Lu, Y., Ferreira, G. C., and Shelnutt, J. A. (2000) Porphyrin interactions with wild-type and mutant mouse ferrochelatase. *Biochemistry 39*, 2517–2529.
34. Balny, C., Anni, H., and Yonetani, T. (1987) A stopped-flow study of the reaction of cytochrome *c* peroxidase with hydroperoxides. *FEBS Lett. 221*, 349–354.

BI702486D